Rotational Resonance Solid-State NMR Elucidates a Structural Model of Pancreatic Amyloid

Janet M. Griffiths,[†,‡,⊥] Ted T. Ashburn,[†] Michèle Auger,[‡,§] Philip R. Costa,[†,‡] Robert G. Griffin,[*,†,‡] and Peter T. Lansbury, Jr.[*,†]

Contribution from the Department of Chemistry and the Francis Bitter National Magnet Laboratory, Massachusetts Institute of Technology, Cambridge, Massachusetts 02139-4307

Received July 19, 1994[⊗]

Abstract: Rotational resonance (R^2) solid-state NMR spectroscopy was used to measure six intercarbon distances in amyloid fibrils comprising ^{13}C-labeled analogs of a peptide (AcHN-SNNFGAILSS-$CONH_2$, $IAPP^H(20-29)$) based on residues 20–29 of the human islet amyloid polypeptide (amylin, $IAPP^H$). The intramolecular intercarbon distances, which constrain the peptide backbone dihedral angles (ϕ, ψ), suggest that $IAPP^H(20-29)$ adopts a highly pleated β sheet structure in the amyloid fibril. This structure is more compact than the antiparallel β sheet model formulated by Pauling to describe the silk fibril. Exaggerated pleating may allow intrastrand van der Waals interactions between hydrophobic side chains. Interstrand interactions can be modeled using qualitative intermolecular R^2 effects which are observed in label dilution experiments. An intermolecular R^2 effect was observed between the C^α of Ala25 and the C=O of Ile26, suggesting their proximity in the amyloid β sheet. The R^2 SSNMR measurements allow the refinement of our two-dimensional model of the $IAPP^H(20-29)$ amyloid β sheet. The refined model may facilitate the design of molecules that bind to pancreatic amyloid. Such molecules may be useful as diagnostics or therapeutics for type-II diabetes.

Introduction

The human islet amyloid polypeptide (amylin, $IAPP^H$)[1,2] is the major component of amyloid deposits which are found in the pancreas of *ca.* 90% of persons with type-II (non-insulin-dependent) diabetes mellitus.[3] Although a causal role has not been proven, the deposition of pancreatic amyloid is strongly associated with the progression and severity of the disease,[4–7] and it is rarely found in non-type-II diabetics.[8,9] A possible role for amyloid in type-II diabetes is suggested by the toxicity of $IAPP^H$ amyloid to pancreatic β-cells.[10] Amyloid fibrils are noncrystalline and have low solubility under physiological conditions. They are, therefore, not amenable to study by traditional structure elucidation techniques (e.g., multidimensional solution ^1H NMR and X-ray crystallography).[11] Solid-state NMR is an ideal technique for the study of amyloid, since insoluble noncrystalline solids can be analyzed. In this study, we use rotational resonance (R^2) solid-state NMR[12,13] to provide structural details of the amyloid formed by a ten amino acid peptide spanning residues 20–29 of $IAPP^H$. The resultant structural model may be useful for the development of therapeutics and diagnostics for type-II diabetes.

The peptide $IAPP^H(20-29)$ (AcHN-SNNFGAILSS-$CONH_2$) forms unbranched fibrils with similar properties to full-length $IAPP^H$.[14–16] Both fibrils exhibit green birefringence after Congo red staining.[17,18] The X-ray fiber diffraction pattern of $IAPP^H(20-29)$ shows reflections at 4.7 and 8.5 Å which are characteristic of β structure (a diffraction pattern for $IAPP^H$ has not been reported).[14,19,20] The presence of a strong absorption band at 1628 cm^{-1} and a weak band at 1695 cm^{-1} in the Fourier transform infrared (FTIR) spectrum of $IAPP^H(20-29)$ suggests that the $IAPP^H(20-29)$ amyloid fibril contains antiparallel β-sheet structure.[21] On the basis of isotope-edited FTIR, we proposed a crude two-dimensional model of the $IAPP^H(20-29)$ amyloid sheet.[21] In our model, the region between Gly24 and Leu27 forms a highly ordered antiparallel β-sheet structure, whereas the termini of the peptide are less ordered. Residues

* Address correspondence to these authors.
† Department of Chemistry.
‡ Francis Bitter National Magnet Laboratory.
§ Current address: Department of Chemistry, Laval University, Quebec City, Quebec, Canada.
⊥ Current address: Department of Chemical Engineering, Massachusetts Institute of Technology.

⊗ Abstract published in *Advance ACS Abstracts*, February 15, 1995.

(1) Abreviations: HFIP, Hexafluoro-2-propanol; IAPP, islet amyloid polypeptide; FTIR, Fourier transform infrared spectroscopy; MAS, magic angle spinning; R^2, rotational resonance.

(2) Nishi, M.; Sanke, T.; Nagamatsu, S.; Bell, G. I.; Steiner, D. F. *J. Biol. Chem.* **1990**, *265*, 4173.
(3) Westermark, P.; Wilander, E. *Diabetologia* **1978**, *15*, 417.
(4) Johnson, K. H.; O'Brein, T. D.; Jordan, K.; Westermark, P. *Am. J. Pathol.* **1989**, *135*, 245.
(5) O'Brien, T. D.; Hayden, D. W.; Johnson, K. H.; Stevens, J. B. *Vet. Pathol.* **1985**, *22*, 250.
(6) Maloy, A. L.; Longnecker, D. S.; Greenberg, E. R. *Hum. Pathol.* **1981**, *12*, 917.
(7) Westermark, P.; Grimerlius, L. *Upsala J. Med. Sci.* **1972**, *77*, 91.
(8) Clark, A.; Lewis, C. E.; Willis, A. C.; Cooper, G. J. S.; Morris, J. F.; Reid, K. B. M.; Turner, R. C. *The Lancet* **1987**, *2*, 231.
(9) Clark, A.; Wells, C. A.; Buley, I. D.; Cruickshank, K. C. J.; Vanhegan, R. I.; Hockaday, T. D. R.; Turner, R. C. *Diabetologia* **1986**, *29*, 528.
(10) Lorenzo, A.; Razzaboni, B.; Weir, G. C.; Yankner, B. A. *Nature* **1994**, *368*, 756.
(11) Lansbury, P. T., Jr. *Biochemistry* **1992**, *31*, 6865.
(12) Levitt, M. H.; Raleigh, D. P.; Creuzet, F.; Griffin, R. G. *J. Chem. Phys.* **1990**, *92*, 6347.
(13) Raleigh, D. P.; Creuzet, F.; Das Gupta, S. K.; Levitt, M. H.; Griffin, R. G. *J. Am. Chem. Soc.* **1989**, *111*, 4502.
(14) Glenner, G. G.; Eanes, D.; Wiley, C. *Biochem. Biophys. Res. Commun.* **1988**, *155*, 608.
(15) Betsholtz, C.; Svensson, V.; Rosman, F.; Engstrom, R.; Westermark, G. T.; Willander, E.; Johnson, K. H.; Westermark, P. *Exp. Cell Res.* **1989**, *183*, 484.
(16) Westermark, P.; Engstrom, U.; Johnson, K. H.; Westermark, G. T.; Betsholtz, C. *Proc. Natl. Acad. Sci. U.S.A.* **1990**, *87*, 5036.
(17) Betsholtz, C.; Christmansson, L.; Engstrom, U.; Rosman, F.; Svensson, V.; Johnson, K. H.; Westermark, P. *FEBS Lett.* **1989**, *251*, 261.
(18) Betsholtz, C.; Christmanson, L.; Engstrom, U.; Rorsman, F.; Jordan, K.; O'Brein, T. D.; Murtaugh, M.; Johnson, K. H.; Westermark, P. *Diabetes* **1990**, *39*, 118.
(19) Fraser, P. E. Personal communication.
(20) Marsh, R. E.; Corey, R. B.; Pauling, L. *Biochim. Biophys. Acta* **1955**, *16*, 1.
(21) Ashburn, T. T.; Auger, M.; Lansbury, P. T., Jr. *J. Am. Chem. Soc.* **1992**, *114*, 790.

0002-7863/95/1517-3539$09.00/0

$$H_2N\text{-}KCNTATCATQRLANFLVHS\underline{SNNFGAILSS}TNVGSNTY\text{-}CONH_2$$

(1, 20, 29, 37)

Figure 1. The primary structure of the human islet amyloid polypeptide ($IAPP^H$). A disulfide bond exists between residues Cys2 and Cys7. The underlined residues (20–29) are modeled by the peptide studied herein.[14,15,16,21]

Ala25 and Ile26 are proximal to one another in the intermolecular sense.[21] A refined model of $IAPP^H(20-29)$, based on R^2 SSNMR studies, is presented herein.

Rotational resonance SSNMR spectroscopy is a technique that measures internuclear distances in solids. The physical basis of R^2 is the measurement of the magnetic dipole–dipole interaction. The strength of this interaction is proportional to $1/r^3$, where r is the distance between two nuclear spins. Although the direct dipole–dipole interaction is normally attenuated during magic angle spinning (MAS), it can be reintroduced under specific experimental conditions. For an isolated pair of ^{13}C nuclei, accurate internuclear distances as great as 6.5 Å can be measured to within 0.1 Å.[13,22–24] R^2 has been applied to a broad variety of solid-state systems including membrane-bound α-helical peptides,[25] the integral membrane protein bacteriorhodopsin,[24,26] and an amyloid fibril comprising a peptide spanning the 9 C-terminal amino acids (β34–42) of the β-amyloid protein of Alzheimer's disease.[23,27] Because crystalline samples are not required, R^2 is particularly well-suited for structural studies of amyloid fibrils.

Experimental Section

Materials. N-Fmoc amino acids were purchased from Advanced Chemtech (Louisville, KY). ^{13}C-labeled amino acids (99% enriched) were purchased from Cambridge Isotopes. All reagents, unless otherwise noted, were obtained from commercial sources.

Peptide Synthesis, Purification, and Characterization. Syntheses were performed using (9-fluorenylmethoxy)carbonyl (Fmoc) amine protection and benzotriazol-1-yl-oxy-tris(pyrrolidino)phosphonium hexafluorophosphate (PyBOP) couplings. The Rink amide 4-(2′,4′-dimethoxyphenyl-Fmoc-aminomethyl)-phenoxyacetamido-norleucyl-MBHA resin (Novabiochem) provided the C-terminal amide and the N-terminus was acetylated with acetic anhydride. Serine (*tert*-butyl) and asparagine (trityl) were deprotected and the peptides were cleaved from resin using a published procedure.[28] Peptides were purified by isocratic reversed-phase high-pressure liquid chromatography (RPHPLC) on a YMC C18 column (300 Å pore size, 15 μm particle size, 30 × 300 mm). Each peptide was judged to be >98% pure and indistinguishable from $IAPP^H(20-29)$[21] by isocratic analytical RPHPLC (Waters C4 column (300 Å, 3.9 × 30 mm)). A single parent ion corresponding to $M + H^+$ was observed in the FAB mass spectrum of each peptide, and the fragmentation pattern verified the sequence and ^{13}C-label positions. Labeled peptides will be designated herein according to the site of labeling, i.e., G^1A^2 contains ^{13}C at the carbonyl carbon (carbon 1) of Gly24 and the α carbon (2) of Ala25. The G^1A^2 peptide was used to measure the 24, α25 distance (vide infra).

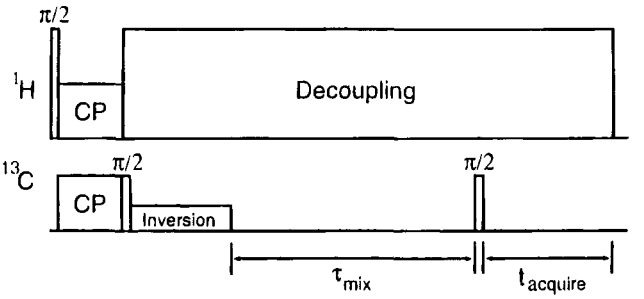

Figure 2. Initial ^{13}C magnetization is generated with a 2 ms cross-polarization pulse. A DANTE inversion[40,41] sequence inverts one resonance line in order to establish a non-equilibrium population condition. Longitudinal magnetization is created with a π/2 pulse. Magnetization exchange takes place for a variable mixing time, τ_m. Data are recorded by adjusting τ_m in discrete steps from 0 to 30 ms. Strong proton decoupling is applied during mixing and acquisition. RF pulses are phase cycled according to an XY-8 scheme.

Preparation of $IAPP^H(20-29)$ Double ^{13}C-Labeled Analogs for Rotational Resonance SSNMR. Samples diluted 10:1 with natural abundance peptide were prepared by dissolving 70 mg of natural abundance $IAPP^H(20-29)$ and 7 mg of double ^{13}C-labeled analog in HFIP. Water was added, the HFIP was removed under reduced pressure, and the aqueous peptide suspension was lyophilized.

R^2 Methodology. The nuclear magnetic dipole–dipole interaction is reintroduced to the NMR spectrum if the sample spinning frequency, ω_r, is chosen to satisfy the condition $\Delta\delta = n\omega_r$ where $\Delta\delta$ is the difference in the isotropic chemical shifts of two labeled nuclei and n is a small integer specifying the order of the resonance. The frequency-selective nature of the R^2 dipolar recoupling condition limits interference due to uncoupled resonances, and therefore permits detection of dipolar couplings between individual spin pairs with a high degree of accuracy.

The R^2 pulse sequence is shown in Figure 2, where the two spectral lines are designated I_{z1} and I_{z2}. An inversion pulse is used to create a population inbalance between the two spins, and hence to facilitate detection of the exchange of magnetization that takes place via the dipole–dipole coupling. The extent of magnetization exchange is recorded for a number of discrete mixing times, usually in the range of 0–30 ms. A zero time point ($\tau_{mix} = 0$) was intercalated between each finite mixing time. After Fourier transformation, the two resonance lines were integrated, summed, and normalized to the average of the two flanking $\tau_{mix} = 0$ data points yielding a difference magnetization $\langle I_{z1} - I_{z2} \rangle$ curve.

Two sets of experiments were performed for each labeled $IAPP^H(20-29)$ analog. An initial data set was recorded for the sample wherein all molecules in the aggregate were doubly ^{13}C labeled at specific sites. These samples are hereafter referred to as "undilute" $IAPP^H(20-29)$. Identical experiments were performed for each double-labeled analog diluted with 10 parts of natural abundance $IAPP^H(20-29)$. These analogs are referred to as "dilute" samples. Fourier transformed spectra of each dilute sample were subtracted from the ^{13}C spectra of unlabeled peptide (^{13}C occurs with a natural abundance level of 1.1%) yielding a set of difference spectra that display two resonance lines corresponding to the two ^{13}C selectively labeled sites. These spectral lines were then integrated, summed, and normalized as descibed above. This procedure yields spectral intensities that are normalized for the extent of R^2 exchange as a function of τ_m.

In order to interpret the R^2 data, a theoretical simulation of magnetization exchange was generated and compared to the experimental exchange curves. The theoretical model depends most strongly on the magnitude of the dipolar coupling interaction. Several orientation and relaxation parameters are also important and can be obtained by careful measurement or estimation. The chemical shift tensor elements of individual spectral lines were measured from slow spinning ^{13}C

(22) Griffiths, J. G.; Griffin, R. G. *Anal. Chim. Acta* **1993**, *283*, 1081.
(23) Spencer, R. G. S.; Halverson, K. H.; Auger, M.; McDermott, A. E.; Griffin, R. G.; Lansbury, P. T., Jr. *Biochemistry* **1991**, *30*, 10382.
(24) Creuzet, F.; McDermott, A.; Gebhard, R.; van der Hoef, K.; Spijker-Assink. M. B.; Herzfeld, J.; Lugtenberg, J.; Levitt, M. H.; Griffin, R. G. *Science* **1991**, *251*, 783.
(25) Peersen, O. B.; Yoshimura, S.; Hojo, H.; Aimoto, S.; Smith, S. O. *J. Am. Chem. Soc.* **1992**, *114*, 4332.
(26) Thompson, L., K.; McDermott, A. E.; Raap, J.; van der Wielen, C. M.; Lugtenburg, J.; Herzfeld, J.; Griffin, R. G. *Biochemistry* **1992**, *31*, 7931.
(27) Lansbury, P. T., Jr.; Costa, P. R.; Griffiths, J. M.; Simon, E. J.; Auger, M.; Halverson, K. J.; Kocisko, D. A.; Hendsch, Z. S.; Ashburn, T. T.; Spencer, R. G. S.; Tidor, B.; Griffin, R. G. Manuscript submitted for publication.
(28) King, D. S.; Fields, C. G.; Fields, G. B. *Int. J. Peptide Protein Res.* **1990**, *36*, 255.
(29) Ramachandran, G. N.; Sasisekharan, V. *Adv. Protein Chem.* **1968**, *23*, 283.
(30) Ramachandran, G. N.; Kolaskar, A. S.; Ramakrishnan, C.; Sasisekharan, V. *Biochim. Biophys. Acta* **1974**, *359*, 298.

CPMAS spectra.[31] The relative orientation of the dipolar and chemical shift tensors were estimated by analogy to glycylglycine.[32] In practice, the angular dependence is small for the resonance condition $n = 1$ which was used to generate all R^2 data reported herein, and a reasonable estimate of the orientation is adequate. Because zero-quantum relaxation competes with magnetization exchange at R^2, an accurate estimation of its rate is particularly important for distance measurements. The zero-quantum relaxation rate $(T_2^{ZQ})^{-1}$ was estimated by summing the homogeneous line widths of each spectral line.[33] A spin−echo experiment was used to determine the homogeneous contribution of each spectral line; these measurements led to T_2^{ZQ} values in the range of ~1−3 ms.[34] It was important for the R^2 analysis to account for magnetization exchange in the presence of inhomogeneous line broadening, since, for a given spinning rate, not all portions of the spectral lines are truely matched at the R^2 condition. Specifically, a model for the line shapes was assumed and the R^2 simulation was performed from each portion of one line to all portions, in turn, of the other, holding the spinning speed and T_2^{ZQ} constant. This approach was verified for a conformation-independent distance (24, α25) within $IAPP^H(20-29)$.

The accuracy of R^2 distance measurements has been validated by measurements in a number of molecules of known crystal structure and measurements of conformation-independent distances in two amyloid samples ($IAPP^H(20-29)$ and $\beta 34-42^{23}$). The specific errors associated with R^2 measurements are discussed elsewhere.[23,26] The most important sources of error stem from the sensitivity of the dipolar recoupling process to the exact R^2 spinning rate, and from overestimation of $(T_2^{ZQ})^{-1}$. Error bars, which ranged from ±0.05 to ±0.2 Å, were determined on the basis of the scatter in the data and the uncertainty in the measured and estimated parameters associated with each distance measurement.

Distance Measurement Strategy. The rotational resonance technique provides constraints for the dihedral angles ω, ϕ, and ψ through a series of internuclear distance measurements.[23,27] Dihedral angles (ω, ϕ, ψ) define the backbone secondary structure about a given residue. Specifically, the torsional angles ϕ(C−N−C$^\alpha$−C) and ψ(N−C$^\alpha$−C−N) describe the relative orientation of the two amide planes joined by a common C$^\alpha$. These angles are constrained by the distances between C$^\alpha_i$ and C$_{i+1}$=O (α1, 2) (which depends upon the dihedral angle ϕ_{i+1} and the configuration of the intervening i to $i+1$ amide bond ($\omega_{i,i+1}$)) and the distances between C$_i$=O and C$^\alpha_{i+2}$ (1, α3) (which depends on ϕ_{i+1} and ψ_{i+1} as well as intervening amide bond $\omega_{i+1,i+2}$, Figure 5).

NMR Experimental Parameters. ^{13}C R^2 SSNMR experiments were performed on a home-built spectrometer operating at 400 MHz for ^1H and 100 MHz for ^{13}C. Peptide samples were packed in 5-mm rotors (Doty Scientific, SC) and spun at the magic angle at a rate dictated by the $n = 1$ R^2 condition, typically in the range of $\omega_r/2\pi$ = 11.0−13.0 kHz. The sample rotation rate was controlled to within ±3 Hz. Pulse lengths were 4.0 μs or less for ^1H and 4.0 μs for ^{13}C.

Construction of Molecular Models. Molecular models were constructed and theoretical carbon-to-carbon distances were calculated as a function of the dihedral angles ϕ, ψ using CAChe version 2 (Tektronix, Beaverton, OR). Data for the Ramachadran plots was generated using a FORTRAN program that assumes fixed bond lengths and bond angles.[29,30]

Results

R^2 Experimental Procedure. Carbon-13 CPMAS spectra were recorded for six doubly ^{13}C-labeled analogs of $IAPP^H$-(20−29). Each spectrum showed two distinct resonance lines corresponding to the selectively ^{13}C-labeled C=O and C$^\alpha$ sites. The isotropic chemical shifts, δ_j, ranged from 170 to 174 ppm for ^{13}C=O and from 43 to 55 ppm for $^{13}C^\alpha$. The specific values were recorded for singly ^{13}C-labeled analogs of $IAPP^H(20-$

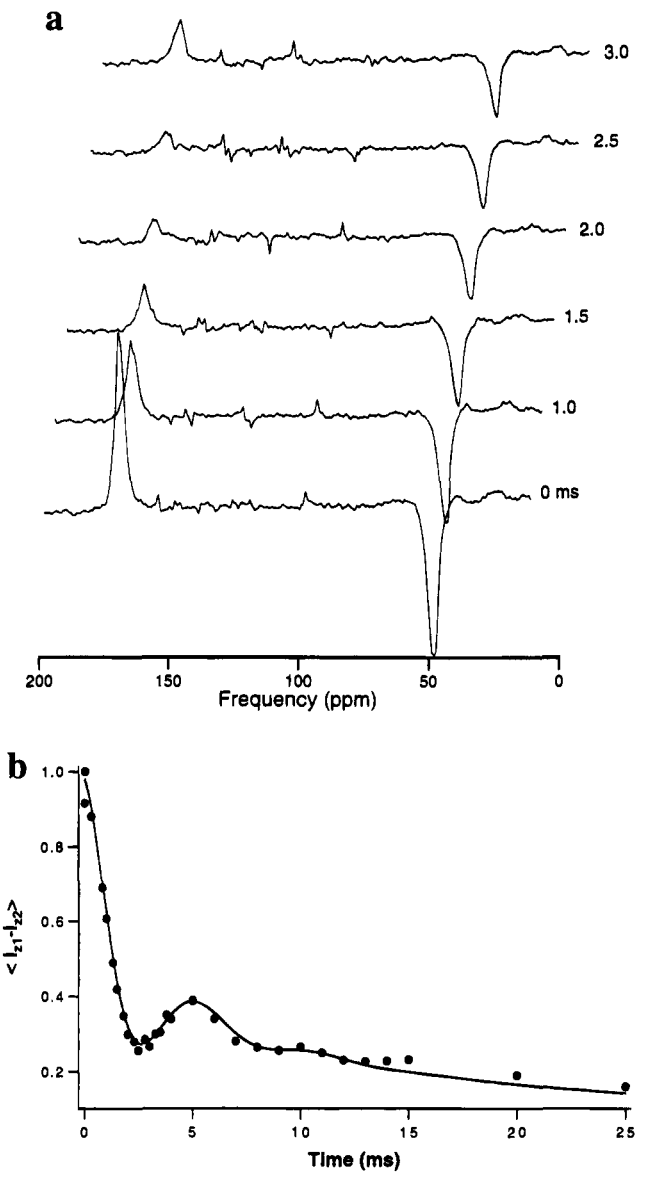

Figure 3. Measurement of 24, α25: (a) The rotational resonance (R^2) magnetization exchange spectra for G^1A^2 showing the change in peak intensities as a function of τ_m. (b) Magnetization exchange data (I) were obtained by integrating and summing peak intensities. A simulation (solid line) corresponding to an intercarbon distance of 2.43 Å is shown. Since the closest possible intermolecular 24, α25 distance is >4 Å, no isotope dilution was performed. The low-intensity peaks between 60 and 160 ppm are due to natural abundance ^{13}C atoms and noise at 0 Hz.

29) in a separate study,[21] and are consistent with the chemical shifts measured in doubly-labeled analogs. The chemical shift difference between labeled sites, $\Delta\delta = \delta_i - \delta_j$, was used to calculate the spinning rate corresponding to the $n = 1$ R^2 condition for each analog. Carbon-13 MAS line widths were also measured for single-labeled $IAPP^H(20-29)$ analogs and ranged from 170 to 200 Hz for ^{13}C=O and from 200 to 400 Hz for C$^\alpha$ atoms.[21] A small increase in line width (≤50 Hz) was observed at the R^2 condition; this observation is consistent with the reintroduction of $^{13}C-^{13}C$ dipolar couplings to the spectrum. Typical spectra are shown in Figure 3a for the G^1A^2 analog (measurement of 24, α25) and in Figure 4a for the A^2I^1 analog (α25, 26). In both cases, the $^{13}C^\alpha$ line was inverted in preparation for the R^2 experiment. Spinning sidebands are present for the ^{13}C=O, but are not prominent for $^{13}C^\alpha$ owing to the smaller shielding anisotropy of sp^3-hybridized carbon atoms. Unresolved resonance lines attributed to natural abun-

(31) Herzfeld, J.; Berger, A. E. *J. Chem. Phys.* **1980**, *73*, 6021.
(32) Haberkorn, R. A.; Stark, R. E.; van Willigen, H.; Griffin, R. G. *J. Am. Chem. Soc.* **1981**, *103*, 2534.
(33) Kubo, A.; McDowell, C. A. *J. Chem. Soc. Faraday Trans.* **1988**, *84*, 3713.
(34) Slichter, C. P. *Principles of Magnetic Resonance*, 3rd ed.; Springer-Verlag: New York, 1990.

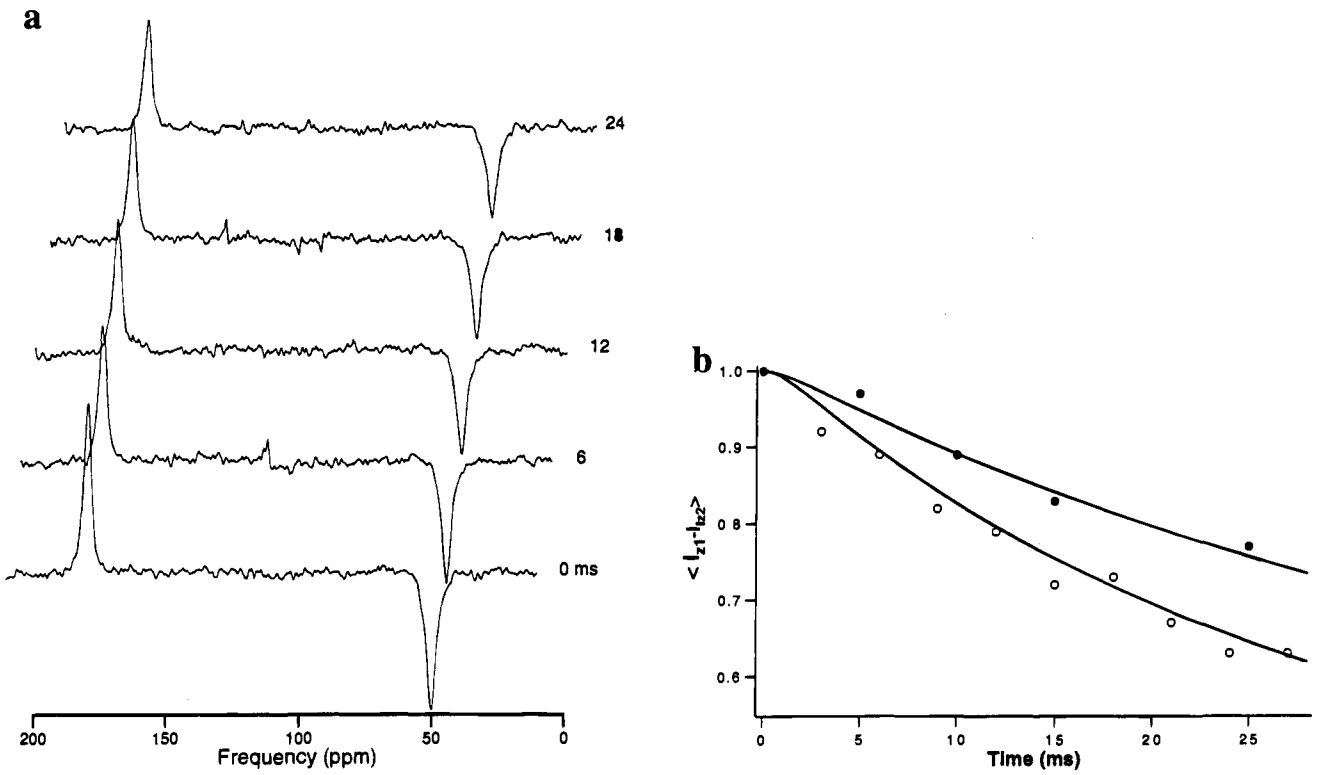

Figure 4. Measurement of α25, 26: (a) The R^2 magnetization exchange spectra of A^2I^1 as a function of τ_m. (b) Experimental and simulated (solid line) magnetization exchange curves for the A^2I^1 fibril. Open circles (○) represent the exchange data for the 100% labeled fibril and correspond to a distance of 4.4 ± 0.1 Å (lower curve). Solid circles (●) represent the exchange data for the 10% labeled fibril and correspond to a distance of 4.8 ± 0.1 Å[42] (upper curve), which represents the intramolecular intercarbon distance. The difference between the two curves represents the intermolecular R^2 effect (8%) which is depicted in Figure 8.

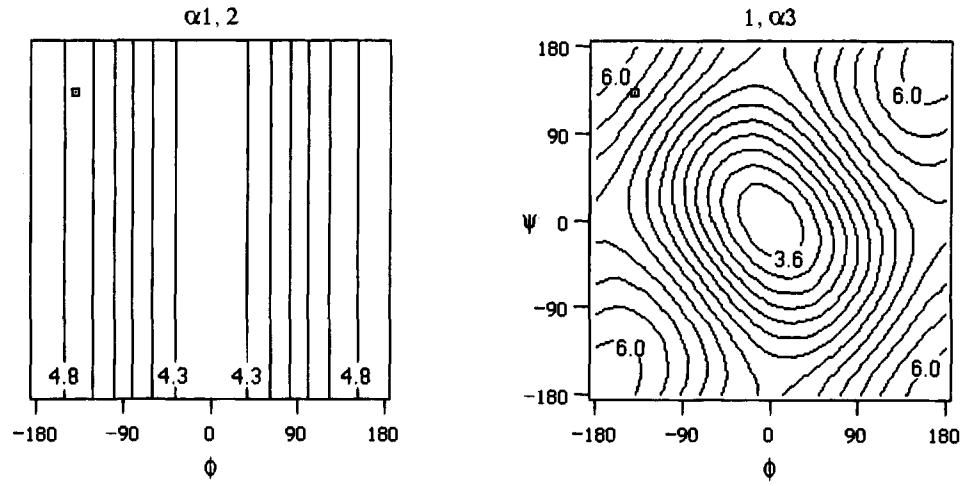

Figure 5. Two measured intercarbon distances constrain conformation space considerably: Ramachandran conformational surfaces with contours showing the relationship between α1, 2 (left) and 1, α3 (right) distances and the dihedral angles ϕ and ψ (assuming trans amide (ω = 180°) geometry).[40] The Pauling antiparallel β sheet/cross-β fibril (−139, 135)[29,30] is indicated by a box in the upper left quadrant.

dance ^{13}C (1.1%) sites are evident in the spectra of dilute and undilute samples. The natural abundance lines are particularly prominent in the dilute samples, but are removed upon subtraction of the labeled and natural abundance $IAPP^H(20-29)$ spectra.

Selectively labeled $^{13}C{=}O$ and $^{13}C^{\alpha}$ resonance lines were generally symmetric and no splittings were observed. Spin–echo measurements, performed at a spinning rate ~1 kHz below the $n = 1$ R^2 condition, were used to delineate homogeneous and inhomogeneous contributions to the measured line width. The homogeneous line widths ($1/\pi T_2$) were typically 50 Hz for $^{13}C{=}O$ sites, and 100 Hz for $^{13}C^{\alpha}$ sites. Possible contributions to the homogeneous line widths include incomplete decoupling and/or dipolar broadening of ^{13}C by the quadrupolar ^{14}N nucleus. The remaining line width was assumed to arise from inhomogeneous broadening sources, such as the presence of a distribution of conformations in the aggregate.[35] Because no large splittings were observed, it is likely that conformational differences in $IAPP^H(20-29)$ are due to the presence, in the amyloid fibril, of a closely related ensemble of conformers. Molecular motion, which can also contribute to line broadening, was ruled out on the basis of chemical shift tensor measurements for the $^{13}C{=}O$ and $^{13}C^{\alpha}$ lines in each $IAPP^H(20-29)$ sample.

Accurate Measure of a Conformation-Independent Intercarbon Distance. Carbon-13 SSNMR exchange spectra,

(35) VanderHart, D. L. *J. Magn. Reson.* **1981**, *44*, 361.

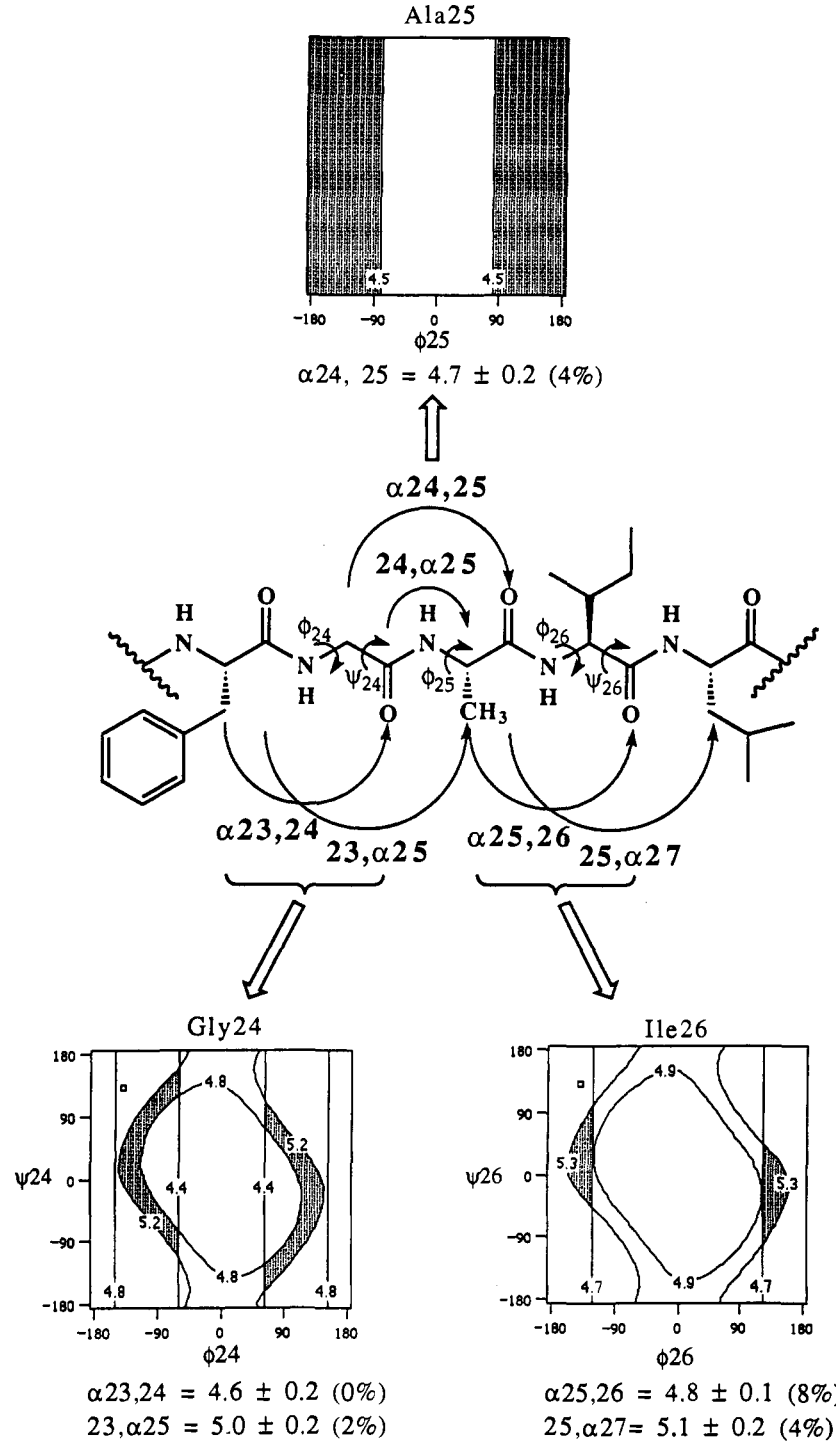

Figure 6. Distance measurements provide information about the local (Gly24-Ile26) conformation. The Ramachandran surfaces are shown for residues Gly24 (lower left), Ala25 (top center), and Ile26 (lower right). The lines on each surface represent the ranges allowed by the R^2 SSNMR measurements. The intersection of the regions allowed by each measurement is shaded; the actual conformation lies within that region. Additional considerations constrain local conformation to a much greater extent than indicated. For each residue, isotope-edited FTIR experiments indicate a local β conformation in the upper left or lower right quadrant. For Ala25 and Ile26, simple energetic considerations rule out conformations in the upper and lower right quadrants.

recorded at the $n = 1$ R^2 condition, are shown in Figure 3a for $IAPP^H(20-29)$ ^{13}C labeled at the C=O carbon of Gly24 and the C^α carbon of Ala25 (analog G^1A^2, distance 24, α25). The corresponding summed intensities are plotted in Figure 3b as a function of mixing time. The 24, α25 intercarbon distance depends only on the geometry of the intervening amide bond, ω24,25 (Figure 6), and is relatively insensitive to amide geometry (cis, $\omega = 0°$, 2.49 Å; trans, $\omega = 180°$, 2.43 Å). The oscillatory decay of $\langle I_{z1} - I_{z2} \rangle$ in Figure 3b arises as a consequence of magnetization exchange among strongly coupled spins. The experimental data are in excellent agreement with the numerical simulation for a distance of 2.43 Å, demonstrating the validity of this methodology (error is *ca.* ±0.05 Å). An additional control distance of 4.5 ± 0.1 Å corresponding to a weak coupling has been measured in a polycrystalline sample of the dipeptide glycylglycine · HCl.[23]

Constraint of the $IAPP^H(20-29)$ Peptide Backbone between Phe23 and Leu27 by Five Intramolecular Distances. Figure 4a shows R^2 spectra of A^2I^1 along with the corresponding intensity plot and simulations in Figure 4b (distance α25, 26;

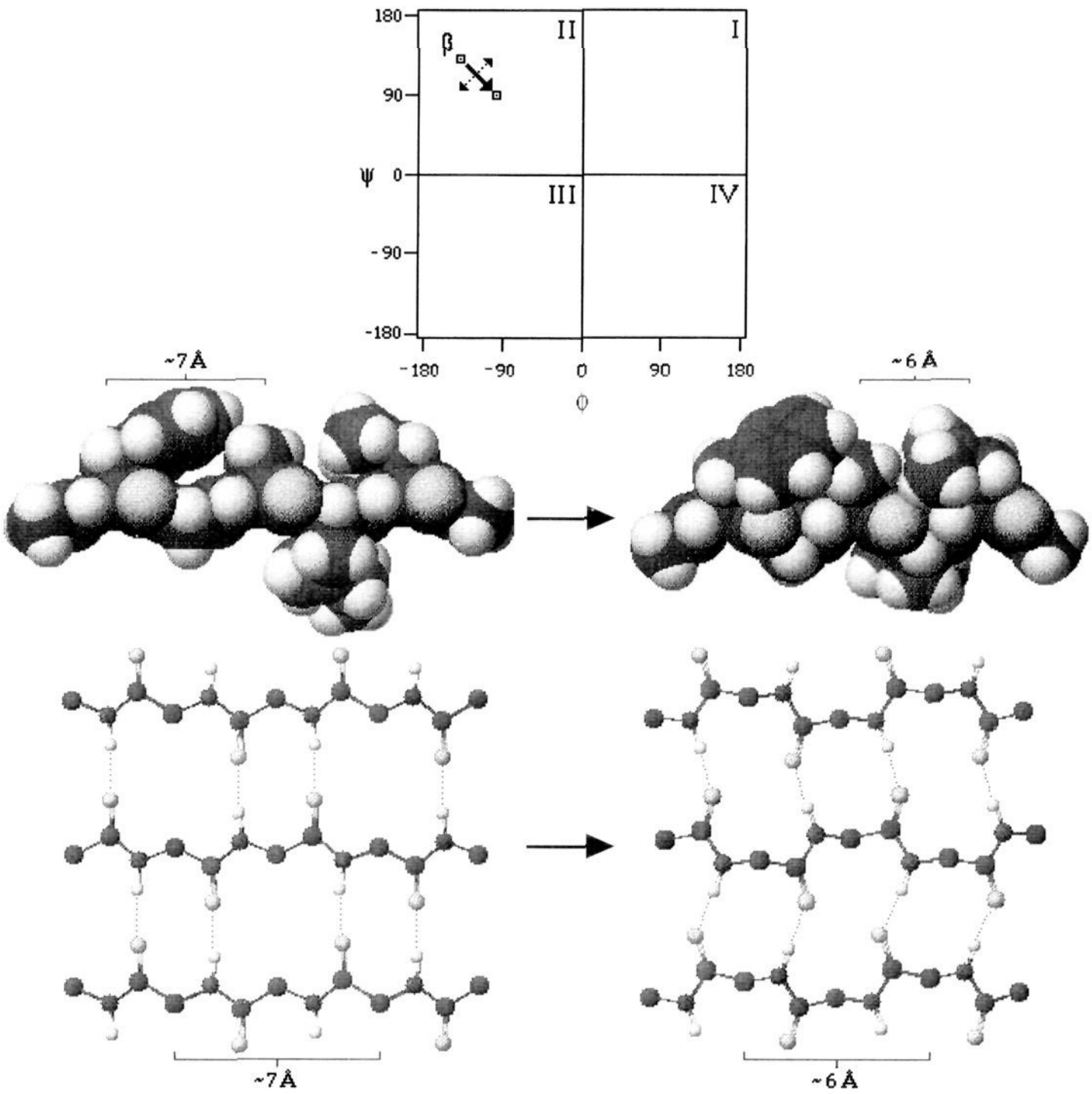

Figure 7. The effect of exaggerated pleating on β sheet structure. (Top) Ramachandran plot showing the difference between the Pauling β strand (β at upper left) and the highly pleated β strand (solid arrow shows pleating). Twisting of the strand,[38] as indicated by the dashed arrow, is not distinguishable by the measurements discussed herein. Untwisted models are presented in this figure and in Figure 8 in order to isolate the consequences of exaggerated pleating. (Middle) Two space-filling models of the Phe23-Leu27 region of $IAPP^H(20-29)$: on the left is the Pauling structure, and on the right, an idealized highly pleated structure ($\phi 23-27$, $\psi 23-27 = -100, 94$). The side chains, about which we have no information, are positioned to illustrate that intrastrand side chain packing can be optimized in the highly pleated β strand. The repeat distance, between the β carbons of Ala25 and Leu27 changes from *ca.* 7 Å in the Pauling β strand at the left to *ca.* 6 Å in the highly pleated β strand at the right. (Bottom) A ball and stick model to show the effect of the exaggerated pleating on the β sheet hydrogen bonding network. Side chains are omitted for clarity. The antiparallel β sheet ((−139, 135), left) was built according to Pauling's specifications.[29,30] The compact sheet model ((−100, 94), right) was built in order to maintain the N-to-O hydrogen bond distance (2.86 Å) and bond angle (180°).

Figure 6). The exchange recorded for the fibrils comprising 100% doubly ^{13}C-labeled peptide results from the combined effects of inter- and intramolecular couplings between ^{13}C-labeled sites. Analysis of fibrils in which *ca.* 10% of peptide is doubly labeled and the remainder is unlabeled, a process we call isotope dilution, measures the intramolecular intercarbon coupling. Both measurements are routinely made. In the example shown in Figure 4, a significant difference exists between the two measurements, indicating that the intermolecular coupling is significant. In these cases, we assume that the two carbons (A^2 and I^1 in Figure 4b) are proximal in the intermolecular, as well as the intramolecular, sense. Because it is possible, yet unlikely, that intermolecular R^2 effects may represent the sum of two separate intermolecular couplings, only qualitative conclusions regarding intermolecular orientation were based on this measurement. In contrast to Figure 3b, no oscillations are present in Figure 4b due to the weak magnitude of the dipolar coupling associated with a longer intercarbon distance.

The six measured intercarbon distances and the five constrained dihedral angles are shown in Figure 6. Two 1, α3 distances, 23, α25 and 25, α27, are significantly shorter than would be predicted for a Pauling antiparallel β sheet ($\phi = -139°$, $\psi = 135°$; square in upper left quadrant; 1, α3 = 5.75 Å, see Figure 5).[29,30] These distances also preclude typical helical structure at G24 and I26 (1, α3 for the three helical conformers is ≤4.7 Å).[28,29] The third 1, α3 distance in this series, 24, α26, was not measured due to the limited availability of singly α-^{13}C-labeled isoleucine. The three measured α1, 2 distances (α23, 24; α24, 25; α25, 26) are greater than 4.4 Å, precluding the possibility of a cis amide bond in this region. The measured distances constrain the relevant dihedral angles according to the Ramachandran surfaces shown in Figure 5. The allowed regions of conformational space for residues G24, A25, and I26 (shaded area in Figure 6) do not take into consideration FTIR data or energetic considerations, both of which further constrain the conformational possibilities.

Observation of Intermolecular R^2 Effects. The extent of

intermolecular coupling was assessed by comparing the dipole coupling before and after isotope dilution. It should be emphasized that, since the "dilution effects" are observed in the magnetization exchange curves, they are not subject to the errors which affect the quantitative analysis of these curves. A significant decrease in dipolar coupling upon dilution (expressed in Figure 6 as a percent change in the simulated interatomic distance on label dilution as compared to the measured intramolecular distance) was observed for the α25, 27 measurement (Figure 4, 4.4 to 4.8 Å on dilution, 8%). Small dilution effects were observed for the peptides G^2A^1 (4%), A^1L^2 (4%), and F^1A^2 (2%). No change in coupling was observed after dilution of F^2G^1.

Discussion

It is our goal to develop a general method, based on R^2 SSNMR and isotope-edited FTIR,[21,35] for the elucidation of amyloid structure.[11] R^2 SSNMR provides two kinds of information: intramolecular intercarbon distances define peptide backbone structure and intermolecular intercarbon distances define interpeptide orientation. Both of these types of data are utilized herein to refine our model for $IAPP^H(20-29)$ amyloid, which was based entirely on isotope-edited FTIR.[21]

Figure 5 shows two Ramachandran surfaces, with a superimposed contour plot corresponding to the α1, 2 and 1, α3 distances, respectively, which are measured by R^2 SSNMR. Both of these distances, especially 1, α3, significantly constrain the peptide backbone. However, additional data are required to constrain a residue to one quadrant.[36] Two experimental methods are utilized for this purpose. Isotope-edited FTIR[21,37] is very useful for determining local secondary structure. The amide I absorption frequency can be used to distinguish between helical structure and β structure, allowing a distinction to be made between the β quadrants (upper left and lower right) and the helical quadrants (upper right and lower left). In addition, ^{13}C SSNMR chemical shifts are sensitive to local secondary structure and can also be used to rule out helical or β strand structure.[21]

Figure 6 shows three Ramachandran surfaces, one for each of the three amino acids in the $IAPP^H(20-29)$ amyloid fibril which are constrained by the measurements reported herein: Gly24, Ala25, and Ile26. For each residue, the regions of conformational space allowed according to the measured intercarbon distances are shaded. A25 is poorly constrained due to the fact that 24, α26 could not be measured. The allowed regions of conformation space available to residues 24−26 are actually more limited than depicted in Figure 6, which reflects only the constraints of the R^2 distances. For residues 24−26, ^{13}C chemical shift measurements and isotope-edited FTIR results indicate that the local conformation is β (upper left or lower right quadrants).[21] For A25 and I26, both right quadrants are disallowed on energetic grounds.[29]

Although the precise conformation at G24 and I26 cannot be determined, certain features of that conformation are discernible. Most notably, the allowed β structures are, in both cases, significantly more pleated than the antiparallel β strand which characterizes Pauling's cross-β fibril (Pauling antiparallel β sheet depicted at left in Figure 7). This exaggerated pleating, or "accordian" motion[38] (indicated by the solid arrow in Figure 7), leads to a more compact structure with a repeat distance of *ca.* 6 Å, as opposed to *ca.* 7 Å for the Pauling β strand (Figure 7).[38] This level of pleating (e.g., to *ca.* −100, 94 as shown in Figure 7) would be energetically feasible.[29] We cannot, on the basis of these data, determine if the $IAPP^H(20-29)$ β sheet is also twisted (dashed arrow in Figure 7).[38] However, the consequences of the highly pleated β structure regarding sidechain packing and interstrand hydrogen bonding are independent of twisting.

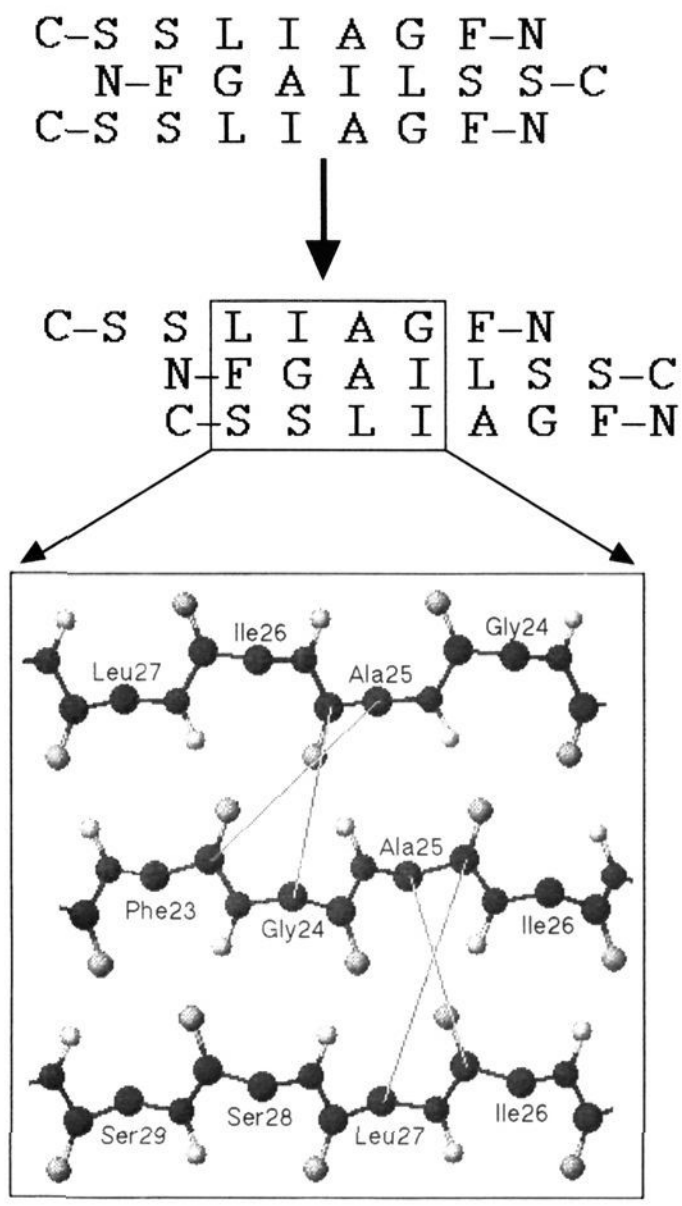

Figure 8. A working model of the F23-S29 section of the $IAPP^H$-(20−29) amyloid β sheet. The model at the top was proposed based solely on isotope-edited FTIR experiments.[21] The revised model is similar, but the interstrand orientations are slightly changed. A section of the revised model is shown at the bottom, in the highly pleated sheet structure which is suggested by the experiments discussed herein. The interstrand lines indicate the four intermolecular R^2 effects which were detected. The shortest measured interstrand distances in the simplified model are as follows: 23, α25, *ca.* 6 Å; α24, 25; *ca.* 5 Å; α25, 26, *ca.* 5 Å; and 25, α27, *ca.* 6 Å. The shortest α23, 24 interstrand distance in this model is >8 Å, consistent with the fact that no intermolecular R^2 effect was observed in that experiment. This model is also consistent with a possible interstrand interaction between the side chains of Phe23 and Ser29[39] and predicts that one face of the $IAPP^H(20-29)$ amyloid β sheet contains the side chains G24, I26, and S28, while the other face contains F23, A25, L27, and S29.

Explanation of Amyloid Insolubility in the Highly Pleated β Sheet Structure. The Pauling cross-β fibril model[20] has been adopted as a general structural model for the amyloid fibril.[11] However, the cross-β fibril was developed to explain the diffraction patterns of silk (predominantly $(Gly\text{-}Ser\text{-}Gly\text{-}Ala)_n$) and polyalanine.[20] This model is not necessarily representative of all amyloid fibrils, which are often rich in large hydrophobic side chains such as Ile and Val.[11]

The increased β sheet pleating of G24 and I26 may reflect a general feature of the entire $IAPP^H(20-29)$ amyloid β sheet. It is therefore instructive to consider the possible effects of exaggerated pleating on amyloid fibril stability. One consequence of the decreased repeat distance (*ca.* 6 Å *vs* 7 Å) relative

(36) Garbow, J. R.; McWherter, C. A. *J. Am. Chem. Soc.* **1993**, *115*, 238.
(37) Halverson, K. J.; Sucholeiki, I.; Ashburn, T. T.; Lansbury, P. T., Jr. *J. Am. Chem. Soc.* **1991**, *113*, 6701.
(38) Salemme, F. R. *Prog. Biophys. Mol. Biol.* **1983**, *42*, 95.

to the Pauling β strand is that the interaction of large side chains at alternating positions in the sequence is possible. The formation of intrastrand hydrophobic clusters, such as the hypothetical one containing F23, A25, and L27 depicted in Figure 7, could stabilize the highly pleated sheet. In contrast, polyalanine and silk (poly(GSGA)) cannot utilize exaggerated pleating to take advantage of intrastrand side chain packing because of the small size of the side chains. However, in the Pauling β sheet, polyalanine is able to efficiently pack via intersheet interactions, in which the "holes" in one sheet are filled with the side chains of the other sheet.[20] This intercalation would not be possible between two highly pleated polyalanine β sheets. We propose that amyloid fibrils rich in Ala and Gly may therefore closely resemble the Pauling cross-β fibril model, whereas those rich in large side chains (e.g., IAPP^H(20−29)) would have a tendency toward exaggerated pleating. The energetic costs of increased pleating are minimal, with respect to both the local conformation[29] and the interstrand hydrogen bond network (Figure 7). Amyloid fibrils comprising a fragment of the β amyloid protein of Alzheimer's disease also contain highly pleated β structure.[27]

Refinement of Our Two-Dimensional Model for IAPP^H-(20−29) Amyloid. The R^2 isotope label dilution experiments detect *inter*molecular dipolar couplings in the aggregate. Because the intersheet distance in the IAPP^H(20−29) amyloid fibril is 8.5 Å,[19] we can rule out the possibility that intermolecular R^2 effects arise from intersheet dipolar coupling. Therefore, these effects allow the refinement of our two-dimensional model of the IAPP^H(20−29) amyloid β sheet. One large intermolecular effect was observed (Figure 4), indicating that Ala25 and Ile26 are proximal in the β sheet.[21] This effect is consistent with our existing model (Figure 8, top), which was based solely on isotope-edited FTIR experiments.[21] However, in order to explain all of the label dilution experiments, the existing model was revised by slightly altering the interstrand orientation (Figure 8, bottom). The revised model is also consistent with data concerning the solubility of IAPP(20−29) sequence variants.[39] Further refinement of this model may allow the design of a molecule which binds to, or inhibits the formation of, IAPP^H amyloid. Such a molecule could have utility as an anti-type-II diabetes diagnostic and/or therapeutic.

Acknowledgment. This work was supported by the National Science Foundation (Presidential Young Investigator Award to P.L., matching donations from Parke-Davis, Genentech, and Merck) and the National Institutes of Health (GM23403 and RR00995 to R.G.). J.M.G. thanks the American Cancer Society for a postdoctoral fellowship. T.T.A. thanks the American Chemical Society (Division of Organic Chemistry) and Procter and Gamble for a graduate fellowship award. M.A. thanks the Natural Sciences and Engineering Research Council of Canada for a postdoctoral fellowship. We also acknowledge Todd S. Anderson, Eric Simon and, especially, Professor Bruce Tidor for valuable discussions related to this work. Thanks also go to B. Q. Sun for the modified R^2 simulation program used herein.

JA942354U

(39) Ashburn, T. T.; Lansbury, P. T., Jr. *J. Am. Chem. Soc.* **1993**, *115*, 11012.

(40) Morris, G. A.; Freeman, R. *J. Magn. Reson.* **1978**, *29*, 433.

(41) Caravatti, P.; Bodenhausen, G.; Ernst, R. R. *J. Magn. Reson.* **1983**, *55*, 88.

(42) The maximum that the α1, 2 and 1, α3 distances may be in a fully extended conformation (ω, ϕ, ψ = 180°) is 4.84 and 6.13 Å, respectively.